

Single and two-particle energy gaps across the disorder-driven superconductor-insulator transition

Karim Bouadim, Yen Lee Loh, Mohit Randeria, and Nandini Trivedi
Department of Physics, The Ohio State University, Columbus, OH 43210, USA

The competition between superconductivity and localization raises profound questions in condensed matter physics. In spite of decades of research, the mechanism of the superconductor-insulator transition (SIT) and the nature of the insulator are not understood. We use quantum Monte Carlo simulations that treat, on an equal footing, inhomogeneous amplitude variations and phase fluctuations, a major advance over previous theories. We gain new microscopic insights and make testable predictions for local spectroscopic probes. The energy gap in the density of states survives across the transition, but coherence peaks exist only in the superconductor. A characteristic pseudogap persists above the critical disorder and critical temperature, in contrast to conventional theories. Surprisingly, the insulator has a two-particle gap scale that vanishes at the SIT, despite a robust single-particle gap.

PACS numbers: 74.40.Kb, 74.62.En, 74.78.-w, 74.81.-g

Attractive interactions between electrons lead to superconductivity, a spectacular example of *long range order* in physics, while disorder leads to *localization* of electronic states. One of the most fascinating examples of the interplay between the effects of interactions and localization is the destruction of superconductivity in thin films with increasing disorder and the resulting superconductor-to-insulator transition (SIT) [1–9].

It was recognized several decades ago that *s*-wave superconductivity (SC) is remarkably robust against weak disorder [10, 11]. It was later argued [12] that SC can survive even when disorder localizes the single-particle states. Thus the superconductor-to-insulator transition must occur in a strong disorder regime that is difficult to treat theoretically in an interacting system. Critical phenomena at the SIT have been described in terms of disordered bosons [13], which model fermion pairs and describe phase fluctuations of the SC order parameter. A more microscopic description must necessarily start with the fermionic degrees of freedom. A Bogoliubov-de Gennes (BdG) treatment of attractive electrons in a random potential shows that the SC pairing amplitude becomes spatially inhomogeneous with strong disorder [14–16]. This leads to a robust energy gap and a large suppression of the superfluid density [14, 15]. However, the phase fluctuations ultimately responsible for the SIT are beyond the BdG approach and are treated in an approximate manner [14, 15, 17].

In this paper we make a major advance using quantum Monte Carlo (QMC) simulations on a fermionic model, which include thermal and quantum fluctuations of the SC phase *and* the spatially inhomogeneous amplitude on an equal footing. While confirming the bosonic mechanism for the SIT, our work also gives new insights into the experimentally observable *electronic* spectral functions. Our results provide us with a detailed description of the phases, the transition, and the quantum critical region at finite temperature.

Our main results are as follows:

- (1) *Single-particle gap*: At $T = 0$ the gap in the single-particle density of states (DOS) survives through the SIT, so that one goes from a gapped superconductor to a gapped insulator. Although the local gap extracted from the local density of states (LDOS) is highly inhomogeneous, it is nevertheless finite at every site.
- (2) *Coherence peaks*: These characteristic pile-ups in the DOS at the gap edges are directly correlated with superconducting order and vanish as the temperature is raised above T_c , or as the disorder is increased across the SIT.
- (3) *Pseudogap*: Near the SIT, a pseudogap – a suppression in the low-energy DOS – persists well above the superconducting T_c up to a crossover temperature scale T^* , in marked deviation from BCS theory. This disorder-driven pseudogap also exists at finite temperatures in the insulating state and grows with disorder.
- (4) *Two-particle gap*: There is a characteristic energy scale ω_{pair} to insert a pair in the insulator that collapses upon approaching the SIT from the insulating side. In addition the two-particle spectral function may also have very small spectral weight at low energies coming from rare regions.

Our predictions for the local tunneling density of states and the dynamical pair susceptibility as a function of temperature and disorder have the potential to guide future experiments using scanning tunneling spectroscopy (STS) [18–21] and other dynamical probes [22].

Model and methods: To model the competition between superconductivity and localization that leads to the SIT in quench-condensed films with thicknesses less than the coherence length, we take the simplest lattice Hamiltonian that has an *s*-wave superconducting ground state in the absence of disorder ($V = 0$) and exhibits Anderson localization when the attractive interaction is turned off ($U = 0$). Thus, we study the two-dimensional

attractive Hubbard model in a random potential:

$$H = -t \sum_{\langle \mathbf{R}\mathbf{R}' \rangle \sigma} (c_{\mathbf{R}\sigma}^\dagger c_{\mathbf{R}'\sigma} + c_{\mathbf{R}'\sigma}^\dagger c_{\mathbf{R}\sigma}) - \sum_{\mathbf{R}\sigma} (\mu - V_{\mathbf{R}}) n_{\mathbf{R}\sigma} - |U| \sum_{\mathbf{R}} n_{\mathbf{R}\uparrow} n_{\mathbf{R}\downarrow}. \quad (1)$$

with lattice sites \mathbf{R} and \mathbf{R}' , spin indices $\sigma = \uparrow$ or \downarrow , fermion creation and annihilation operators $c_{\mathbf{R}\sigma}^\dagger$ and $c_{\mathbf{R}\sigma}$, number operators $n_{\mathbf{R}\sigma} = c_{\mathbf{R}\sigma}^\dagger c_{\mathbf{R}\sigma}$, hopping t between neighboring sites $\langle \mathbf{R}\mathbf{R}' \rangle$, and a chemical potential μ chosen such that the average density is $\langle n \rangle \neq 1$. $V_{\mathbf{R}}$ is a random potential at each site drawn from the uniform distribution on $[-V, +V]$, and $|U|$ is the on-site attraction leading to s -wave SC. We will measure all energies in units of t .

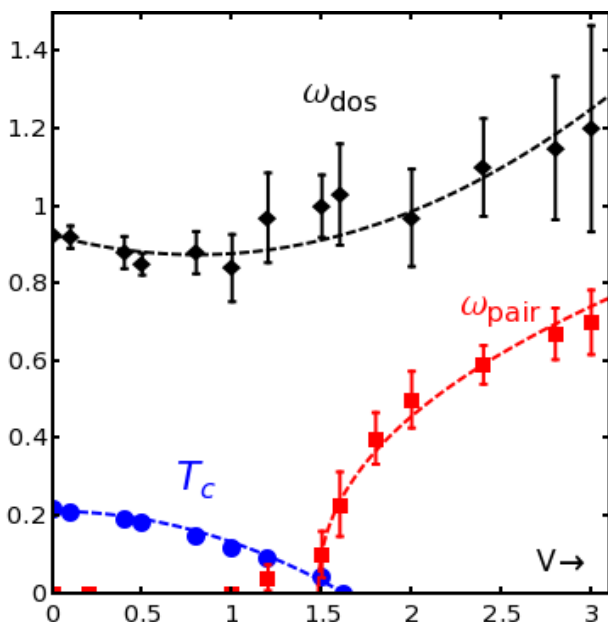


FIG. 1: **Energy and temperature scales across the superconductor-insulator transition (SIT).** The superconducting T_c (blue dots) decreases to zero at the critical disorder strength V_c . The single-particle gap ω_{dos} (black diamonds), obtained from the DOS shown in Fig. 2, is large and finite in all states. The two-particle energy scale ω_{pair} (red squares), obtained from the dynamical pair susceptibility shown in Fig. 3, is non-zero in the insulator but vanishes at the SIT. The dashed curves are guides to the eye; extracting critical exponents requires finite-size scaling beyond the scope of this paper. The statistical error bars in all the figures are dominated by disorder averaging and not from the QMC. These results are obtained at fixed attraction $|U| = 4$ and average density $\langle n \rangle \approx 0.87$ on 10 disorder realizations on 8×8 lattices. ω_{pair} and ω_{dos} are calculated at the lowest accessible temperature, $T = 0.1$. For specific parameter values, we have run extensive simulations that average over 100 disorder realizations.

We use the determinantal QMC method [23], which is free of the fermion sign problem for the Hamiltonian (1).

We choose $|U| = 4$, so that the coherence length is within the system size, and $\langle n \rangle = 0.875$. We have made extensive comparisons of the QMC results with self-consistent BdG calculations, which take into account only the spatial amplitude variations; see supplementary material. These comparisons permit us to separate the effects of amplitude inhomogeneity and phase fluctuations.

We compute frequency-dependent observables across the SIT for the first time. The single-particle DOS, LDOS and the pair susceptibility are obtained using the maximum entropy method (MEM) for analytic continuation [24, 25]. We have verified that these results obey various sum rules to high precision, and that the MEM correctly reproduces the low-energy structure of test spectra as shown in the supplementary material. What gives us confidence is that our central results on the single- and two-particle gaps can be equally well estimated directly from the exponential decay of the imaginary-time QMC data, without recourse to MEM.

Phase diagram: In Fig. 1 we summarize our key results for the disorder dependence of various temperature and energy scales. Since the finite temperature transition is expected to be in the Berezinskii-Kosterlitz-Thouless universality class, we estimate the critical temperature T_c from the superfluid density ρ_s , calculated from the transverse current correlator [26, 27]. We note that this procedure on finite systems provide an upper bound on the actual T_c in the thermodynamic limit. As disorder strength V increases, T_c falls and finally vanishes at the critical disorder V_c , which defines the SIT. The single-particle energy gap ω_{dos} remains non-zero across the SIT, whereas the two-particle energy scale ω_{pair} is finite in the insulator and goes to zero at the transition. These gap scales are extracted from the DOS and the dynamical pair susceptibility discussed in detail below. Figure 1 can be interpreted as a phase diagram: T_c is the superconducting transition temperature, ω_{pair} is a crossover scale between the insulator and the quantum critical region, and ω_{dos} is related to the pseudogap crossover scale described below.

Single-particle spectra: We show in Fig. 2 the disorder and temperature dependence of the DOS $N(\omega)$. Panels (A,B) show the evolution with disorder at a very low temperature $T = 0.1$. The gap ω_{dos} *clearly remains finite* in both superconducting and insulating states, a counter-intuitive observation that agrees qualitatively with BdG results [14, 15]. In contrast, the coherence peaks diminish with increasing V and disappear near the SIT at $V_c \approx 1.6$.

Figures 2(C,D) show the temperature evolution of $N(\omega)$ at weak disorder $V < V_c$. Unlike in BCS theory, the hard SC gap does not close with increasing T . Instead, the coherence peaks gradually disappear as the temperature increases across T_c . Above T_c , the gap gradually fills up, with a pseudogap persisting well above T_c .

The temperature evolution of $N(\omega)$ at strong disorder $V > V_c$ is shown in Fig. 2(E,F). Here the ground state

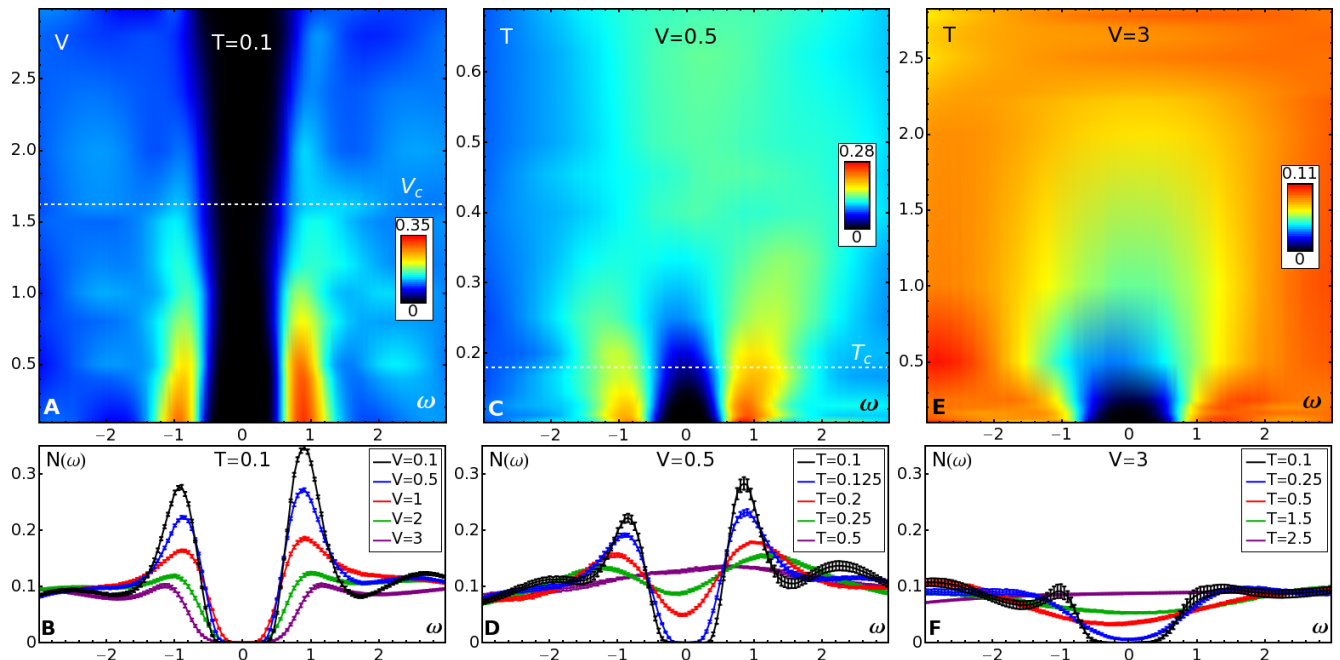


FIG. 2: **The single-particle DOS** $N(\omega)$ (upper panels) and representative spectra (lower panels) along three different cuts through the temperature-disorder plane. Left panels (A,B): Disorder dependence of $N(\omega)$ at a fixed low temperature. A hard gap (black region) persists for all V above and below the SIT ($V_c \approx 1.6$), but the coherence peaks (red) exist only in the SC state and not in the insulator. Center panels (C,D): T -dependence of the $N(\omega)$ for the superconductor ($V < V_c$). The coherence peaks (red) visible in the SC state, vanish for $T \gtrsim T_c \approx 0.14$. A *disorder-induced pseudogap*, with loss of low-energy spectral weight, persists well above T_c . Right panels (E,F): T -dependence of $N(\omega)$ for the insulator ($V > V_c$). The hard insulating gap at low T evolves into a pseudogap at higher T . No coherence peaks are observed at any T . All panels show data averaged over 10–100 disorder realizations.

is an insulator with a hard gap and little evidence for coherence peaks, and the pseudogap persists up to an even higher temperature.

Two-particle spectra: Given that we find an insulator with a single-particle gap, what is the energy scale that vanishes upon approaching the quantum critical point from the insulating side? We propose that it is the typical energy for a *two-particle excitation* in the insulator. To access this scale, we examine the pair susceptibility $P(\omega)$ obtained by analytical continuation of the correlation function $P(\tau) = \sum_{\mathbf{R}} \langle \mathcal{T}_\tau F(\mathbf{R}; \tau) F^\dagger(\mathbf{R}; 0) \rangle$ where $F(\mathbf{R}, \tau) = c_{\mathbf{R}\downarrow}(\tau) c_{\mathbf{R}\uparrow}(\tau)$. Thus $P(\tau)$ is the amplitude for a pair created at a site \mathbf{R} at $\tau = 0$ to be found at the same site at a later time τ . We find that in the insulating phase $P(\tau)$ decays exponentially, which allows us to define ω_{pair} , the characteristic energy scale for two-particle excitations.

In Fig. 3 we show the imaginary part of the pair susceptibility $P''(\omega)/\omega$ for three disorder strengths. At weak disorder $P''(\omega)/\omega$ is very large at low ω , whereas at strong disorder it has a clear two-peak structure with a characteristic energy scale ω_{pair} . This dominant scale represents the typical energy required to insert a pair into the system. We find that ω_{pair} collapses to zero at the SIT because there is no cost for inserting a pair into a

condensate.

At sufficiently small energies our insulating state is similar to a Bose glass, in which rare regions [28] give rise to a very small but non-zero spectral weight in $P''(\omega)/\omega$ at low energies. Such Griffiths-McCoy-Wu singularities can be very difficult to pin down in numerical simulations and even in experiments. Nevertheless, we do indeed see some signs of low-energy spectral weight in, e.g., Fig. 3B. In this paper, however, we focus on the most salient features in $P''(\omega)/\omega$. These are the *peaks* at $\pm\omega_{\text{pair}}$, which imply that the *typical* energy cost to insert a pair is finite.

Local probes: In Fig. 4 we track the behavior of various local quantities with increasing disorder strength V . We show the LDOS $N(\mathbf{R}, \omega)$ at representative points, maps of the spatial variation of the density $n(\mathbf{R})$, and the BdG pairing amplitude $\Delta_{\text{op}}(\mathbf{R}) = \langle c_{\mathbf{R}\downarrow} c_{\mathbf{R}\uparrow} \rangle$ (which cannot be computed in QMC). We see that the system becomes increasingly inhomogeneous with increasing disorder, as we move from left to right in Fig. 4. The SIT occurs due to loss of phase coherence between superconducting islands, seen as blue patches in the map of the pairing amplitude $\Delta_{\text{op}}(\mathbf{R})$.

We predict experimentally measurable signatures of the local density and pairing amplitude in the LDOS $N(\mathbf{R}, \omega)$. Let us focus on three representative sites \mathbf{R}_1 , \mathbf{R}_2 , and \mathbf{R}_3 . At moderate and strong disorder, \mathbf{R}_1 is

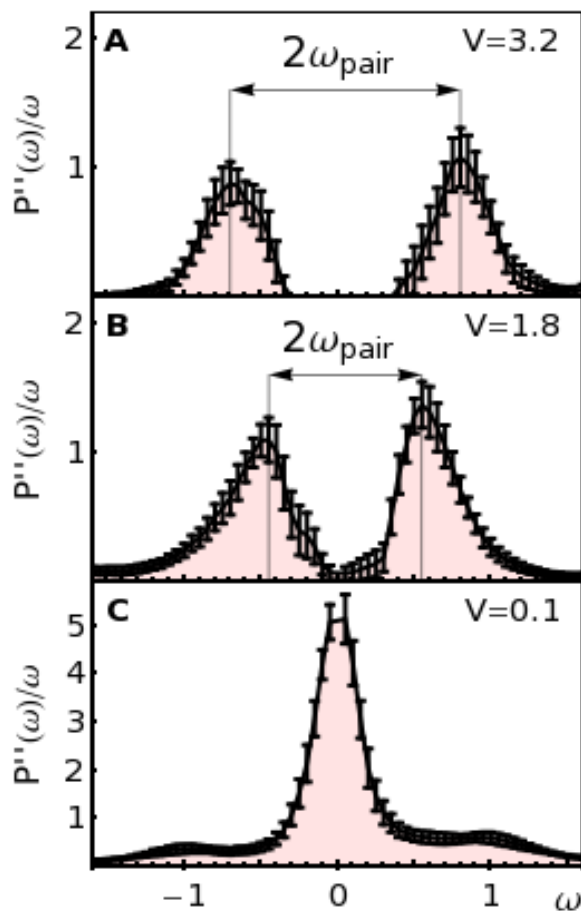


FIG. 3: **Imaginary part of the dynamical pair susceptibility** $P''(\omega)/\omega$ at $T = 0.1t$, averaged over 10 disorder realizations at three disorder strengths. Error bars represent variations between disorder realizations. For $V < V_c$, there is a large peak at $\omega = 0$, indicating zero energy cost to insert a pair into the SC. For $V > V_c$, there is a gap-like structure with an energy scale ω_{pair} , the typical energy required to insert a pair into the insulator which increases with V .

located on a potential hill, with a low density $n(\mathbf{R}_1) \approx 0$ and a negligible pairing amplitude $\Delta_{\text{op}}(\mathbf{R}_1) \approx 0$. Thus the LDOS at \mathbf{R}_1 is highly asymmetric, with most of the spectral weight at $\omega > 0$, for adding an electron. In contrast, \mathbf{R}_3 is in a potential well, with a high density $n(\mathbf{R}_3) \approx 2$ and a negligible pairing amplitude $\Delta_{\text{op}}(\mathbf{R}_3) \approx 0$. Thus \mathbf{R}_3 also has a highly asymmetric LDOS, but most of the spectral weight is at $\omega < 0$, for removing an electron. We believe that MEM correctly captures the gap, coherence peaks, and integrated spectral asymmetry (tested by sum rules); it is much less reliable for high-energy spectral features, which are in any case irrelevant for our purposes.

Finally, \mathbf{R}_2 lies in a superconducting island close to half-filling, $n(\mathbf{R}_2) \approx 1$, which permits particle-hole mixing, and therefore a large pairing amplitude $\Delta_{\text{op}}(\mathbf{R}_2)$. The LDOS at \mathbf{R}_2 is much more symmetrical, with large

coherence peaks that persist across the SIT and even in the insulating state. Note that all the LDOS curves have a clear gap. We thus find that symmetrical coherence peaks in the LDOS, and not the local energy gap, are a clear experimental signature of a local pairing amplitude, which is difficult to probe by other means.

Discussion: We now discuss our results in light of existing theories. We have ignored the renormalization of the effective interaction between electrons arising from changes in screening with increasing disorder [29]. Our point of view is that electronic inhomogeneity (that we focus on) is much more important in the vicinity of the SIT than the disorder dependence of the effective $|U|$ (that we neglect), so long as the latter is *not* driven to zero. This assumption is validated by experiments that find a non-zero gap across the SIT [18].

Our results are consistent with the absence of a fermionic or bosonic metal phase in between the superconductor and the insulator. Although we have not computed transport here (see ref. [27] for an approximate calculation of the resistivity in the same model), we do not find any extended low-energy excitations characteristic of a metallic phase.

The existence of gapped fermions implies a phase-fluctuation-dominated “bosonic” picture for the superconductor-insulator transition [13, 28]. However, we must emphasize that we *did not assume* such a bosonic picture from the outset. A nontrivial aspect of our results is that even though we started with a model of interacting fermions in a random potential and could have, in principle, obtained (localized) gapless fermions in the insulator, we did not find such excitations. The reason all fermionic excitations are gapped is intimately related to the structure of the inhomogeneous local pairing amplitude $\Delta_{\text{op}}(\mathbf{R}) = \langle c_{\mathbf{R}\downarrow} c_{\mathbf{R}\uparrow} \rangle$ generated in the presence of large disorder, as we now explain.

We show in Fig. 5 that even for “homogeneous” disorder, i.e., an uncorrelated random potential $V(\mathbf{R})$ (see panel A), the pairing amplitude $\Delta_{\text{op}}(\mathbf{R})$ exhibits an emergent “granular” structure (shown in panel B). The system self-organizes into superconducting islands, on the scale of the coherence length, with finite $\Delta_{\text{op}}(\mathbf{R})$, interspersed with insulating regions where $\Delta_{\text{op}}(\mathbf{R})$ is negligible. The spatial variations of spectral features (asymmetry and coherence peaks) in this inhomogeneous state were already discussed above in connection with Fig. 4.

The close connection between inhomogeneity and energy gaps is made clear in Figs. 5 B and C which demonstrate two striking facts. We see that (i) there is an energy gap in the LDOS at every site, and (ii) small gaps $\omega_{\text{dos}}(\mathbf{R})$ in the LDOS are spatially correlated with large $\Delta_{\text{op}}(\mathbf{R})$ SC islands.

A simple way to understand these results is to use the pairing-of-exact-eigenstates approach generalized to highly disordered systems [15]. In the limit of weak attraction, pairing gaps out the low-energy density of states

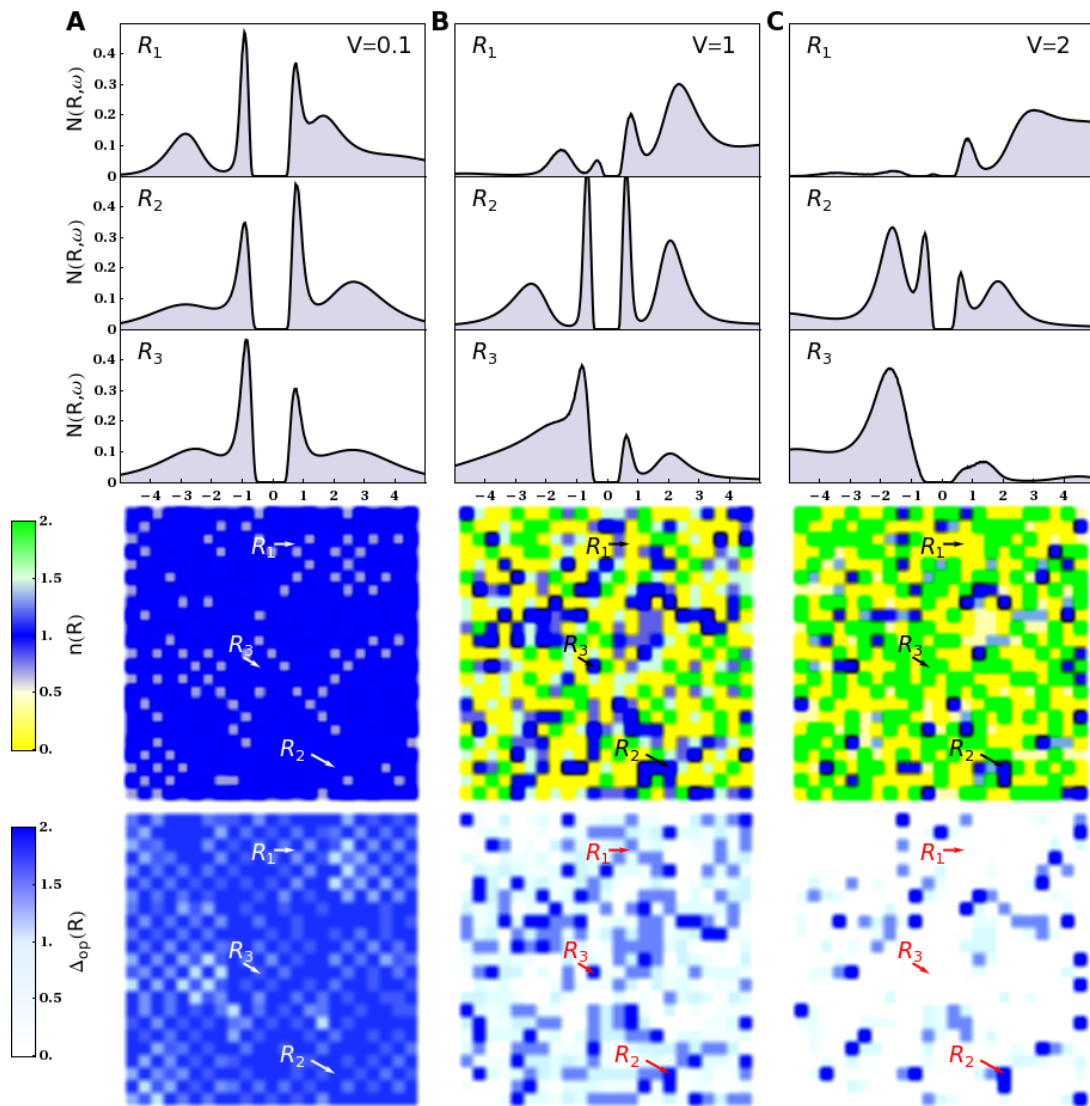


FIG. 4: Local density of states (LDOS) $N(\mathbf{R}, \omega)$, density $n(\mathbf{R})$, and BdG pairing amplitude $\Delta_{\text{op}}(\mathbf{R})$ as a function of disorder strength for a montage of nine disorder realizations of 8×8 lattices. Panels A, B, C correspond to $V = 0.1, 1, 2$ respectively. The LDOS is plotted at three representative sites \mathbf{R}_i . At moderate and strong disorder, site \mathbf{R}_1 is on a high potential hill that is nearly empty, and \mathbf{R}_3 is in a deep valley that is almost doubly occupied. This leads to the characteristic asymmetries in the LDOS in the center and right columns for \mathbf{R}_1 and \mathbf{R}_3 . The small local pairing amplitude $\Delta_{\text{op}}(\mathbf{R})$ at these two sites is reflected in the absence of coherence peaks in the LDOS. In contrast, site \mathbf{R}_2 has a density closer to half-filling, leading to a significant local pairing amplitude, a much more symmetrical LDOS, and coherence peaks that persist even at strong disorder.

in the underlying Anderson insulator and leads to the islands with non-zero Δ_{op} and a small energy gap. On the other hand, the insulating sea corresponds to the higher-energy strongly localized states in the system.

From this perspective one can see that the gap ω_{dos} , observed in the spatially average DOS, initially decreases with increasing disorder due to a reduction in the density of states near the chemical potential in our model. (In a real material, the coupling will also decrease [29] with disorder). However, at high disorder, the gap *grows* (consistent with Fig. 1) like $\omega_{\text{dos}} \approx |U|/(2\xi_{\text{loc}}^2)$ where ξ_{loc} is the single-particle localization length [15]. This is due to

the enhanced effective attraction between fermions confined to a smaller localization volume ξ_{loc}^2 .

The phase stiffness (or superfluid density) $\rho_s(T = 0)$, on the other hand, decreases monotonically with disorder as the SC islands become smaller and the Josephson coupling between islands becomes weaker. Thus, even if one starts with a weak-coupling BCS superconductor with $\omega_{\text{dos}} \ll \rho_s$, disorder will necessarily drive it into the $\omega_{\text{dos}} \gg \rho_s$ regime. Eventually quantum phase fluctuations destroy long-range order at $T = 0$, leading to an insulator whose low-energy excitations are pairs localized on SC islands.

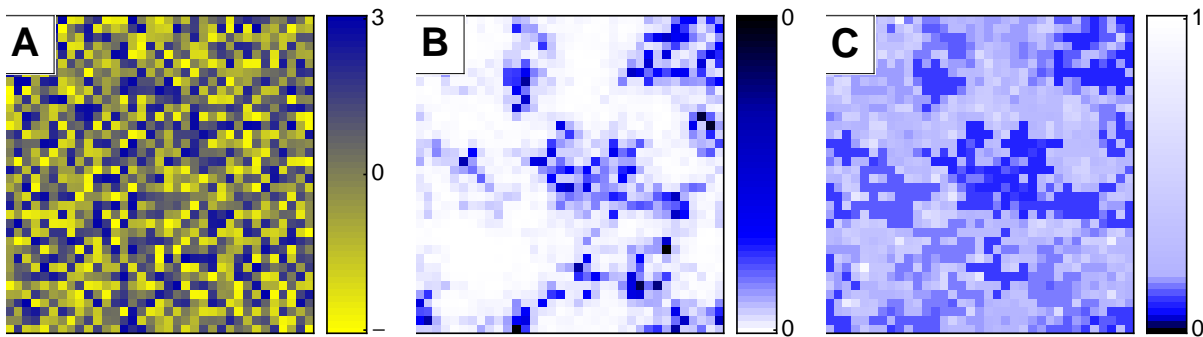


FIG. 5: **Emergent granularity:** (A) Disorder realization $V(\mathbf{R})$ on a 36×36 lattice at $V = 3t$. (B) Local pairing amplitude $\Delta_{\text{op}}(\mathbf{R})$ from a BdG calculation at $|U| = 1.5t$, $T = 0$, and $n = 0.875$. Note the emergent “granular” structure where the pairing amplitude “self-organizes” into superconducting islands on the scale of the coherence length, even though the “homogeneous” disorder potential in (A) varies on the scale of a lattice spacing. (C) Local energy gap $\omega_{\text{dos}}(\mathbf{R})$ from BdG, defined as the smallest energy at which the local DOS is non-zero ($N(\mathbf{R}, \omega) > 0.004$). Note that this gap is finite everywhere and *smallest gaps* occur on the SC islands defined by the *largest pairing amplitude*.

The low- ρ_s regime on the SC side of the SIT leads to a finite-temperature transition driven by thermal phase fluctuations [30] with $T_c \sim \rho_s(0)$. The large energy gap then leads to a marked deviation from conventional BCS theory, with a pairing pseudogap in the temperature range $T_c \lesssim T \lesssim \omega_{\text{dos}}$. This pseudogap exists even in the weak-coupling regime, provided one is close enough to the SIT so that $\rho_s \ll \omega_{\text{dos}}$.

Comparison with experiments: We describe the connection between our predictions and experiments on the disorder-tuned SIT in systems such as indium oxide, titanium nitride, and niobium nitride films, for which our theory seems to be the most appropriate. First let us discuss the insulating side of the SIT. The existence of a gap in the insulator implies activated transport, consistent with early measurements on amorphous InO_x films [5]. In addition, there is evidence for pairs on the insulating side of the transition [8] in specially patterned amorphous bismuth films.

Recent STM experiments are directly relevant to our predictions on the superconducting side of the SIT. Experiments on homogeneously disordered TiN films [18] have shown that, while T_c goes to zero at the SIT, the STM gap ω_{dos} remains finite, in agreement with Fig. 1. In addition, the gap in the LDOS shows significant inhomogeneity, which supports our picture of emergent granularity (see Figs. 4 and 5). After our paper was written, we became aware of new experiments that corroborate our predictions. STM experiments on InO_x [31], TiN [32], and NbN films [33] have all found a pseudogap persisting up to many times T_c . In particular, they observe a marked suppression of the low-energy DOS together with a destruction of coherence peaks above T_c , in complete agreement with our predictions.

We hope that future STM experiments will study in detail the anticorrelation that we predict between the

height of the coherence peaks (associated with large pairing amplitude) and the small energy gaps in the local DOS. The obvious quantum critical scaling between T_c and $\rho_s(0)$ at the SIT, well studied in rather different systems [34], also remains to be tested experimentally in s -wave superconducting films.

Conclusion: In conclusion, we have obtained detailed insights and predictions for observable properties of the highly disordered superconducting and insulating states in 2D films, and of the transition between these states. Although we focused on s -wave SC films, it has not escaped our attention that aspects of our results bear a striking resemblance to the completely different – and much less understood – problem of the pseudogap in the d -wave high T_c superconductors. Features like the loss of low-energy spectral weight persisting across thermal or quantum phase transitions, even as coherence peaks are destroyed, may well be common to all systems where the small superfluid stiffness drives the loss of phase coherence. The pseudogap in underdoped cuprates is driven by the proximity to the Mott insulator and further complicated by competing order parameters, with disorder probably playing a secondary role, unlike the disorder-induced pseudogap near the SIT discussed in this paper.

Correspondence and request for materials should be addressed to: N. Trivedi (trivedi.15@osu.edu).

We gratefully acknowledge support from NSF DMR-0907275 (KB), US Department of Energy, Office of Basic Energy Sciences grant DOE DE-FG02-07ER46423 (NT, YLL), NSF DMR-0706203 and NSF DMR-1006532 (MR), and computational support from the Ohio Supercomputing Center. KB and YLL performed the numerical calculations; MR and NT were responsible for the project planning; KB, YLL, MR and NT contributed to the data analysis, discussions and writing.

-
- [1] Goldman, A. and Markovic, N. Superconductor-insulator transitions in the two-dimensional limit. *Physics Today* **51**, 39–44 (1998).
- [2] Gantmakher, V. F. and Dolgoplov, V. T. Superconductor-insulator quantum phase transition. *Physics-Uspexhi* **53**, 3–53 (2010).
- [3] Haviland, D. B., Liu, Y., and Goldman, A. M. Onset of superconductivity in the two-dimensional limit. *Physical Review Letters* **62**(18), 2180–2183 (1989).
- [4] Hebard, A. F. and Paalanen, M. A. Magnetic-field-tuned superconductor-insulator transition in two-dimensional films. *Physical Review Letters* **65**(7), 927–930 (1990).
- [5] Shahar, D. and Ovadyahu, Z. Superconductivity near the mobility edge. *Physical Review B* **46**(17), 10917–10922 (1992).
- [6] Adams, P. W. Field-induced spin mixing in ultra-thin superconducting Al and Be films in high parallel magnetic fields. *Physical Review Letters* **92**(6), 067003 (2004).
- [7] Steiner, M. A., Boebinger, G., and Kapitulnik, A. Possible field-tuned superconductor-insulator transition in high- T_c superconductors: Implications for pairing at high magnetic fields. *Physical Review Letters* **94**(10), 107008 (2005).
- [8] Stewart, M. D., Yin, A., Xu, J. M., and Valles, J. M. Superconducting pair correlations in an amorphous insulating nanohoneycomb film. *Science* **318**, 1273–1275 (2007).
- [9] Sachdev, S. *Quantum Phase Transitions*. Cambridge, London, (1999).
- [10] Anderson, P. W. Theory of dirty superconductors. *Journal of Physics and Chemistry of Solids* **11**, 26–30 (1959).
- [11] Abrikosov, A. A. and Gor'kov, L. P. Superconducting alloys at finite temperatures. *Zhurnal Eksperimental'noi i Teoreticheskoi Fiziki* **36**, 319–320 (1959) [*Soviet Physics Journal of Experimental and Theoretical Physics* **9**, 220–221 (1959)].
- [12] Ma, M. and Lee, P. A. Localized superconductors. *Physical Review B* **32**(9), 5658–5667 (1985).
- [13] Fisher, M. P. A., Grinstein, G., and Girvin, S. M. Presence of quantum diffusion in two dimensions: Universal resistance at the superconductor-insulator transition. *Physical Review Letters* **64**(5), 587–590 (1990).
- [14] Ghosal, A., Randeria, M., and Trivedi, N. Role of spatial amplitude fluctuations in highly disordered s-wave superconductors. *Physical Review Letters* **81**(18), 3940–3943 (1998).
- [15] Ghosal, A., Randeria, M., and Trivedi, N. Inhomogeneous pairing in highly disordered s-wave superconductors. *Physical Review B* **65**(1), 014501 (2001).
- [16] Feigel'man, M. V., Ioffe, L. B., Kravtsov, V. E., and Yuzbashyan, E. A. Eigenfunction fractality and pseudogap state near the superconductor-insulator transition. *Physical Review Letters* **98**(2), 027001 (2007).
- [17] Dubi, Y., Meir, Y., and Avishai, Y. Nature of the superconductor-insulator transition in disordered superconductors. *Nature* **449**(7164), 876–880 (2007).
- [18] Sacépé, B., Chapelier, C., Baturina, T. I., Vinokur, V. M., Baklanov, M. R., and Sanquer, M. Disorder-induced inhomogeneities of the superconducting state close to the superconductor-insulator transition. *Physical Review Letters* **101**(15), 157006 (2008).
- [19] Cren, T., Roditchev, D., Sacks, W., Klein, J., Moussy, J.-B., Deville-Cavellin, C., and Laguès, M. Influence of disorder on the local density of states in high- t_c superconducting thin films. *Physical Review Letters* **84**(1), 147–150 (2000).
- [20] Lang, K. M., Madhavan, V., J, E. H., Hudson, E. W., Eisaki, H., Uchida, S., and Davis, J. C. Imaging the granular structure of high- T_c superconductivity in underdoped $\text{Bi}_2\text{Sr}_2\text{CaCu}_2\text{O}_{8+\delta}$. *Nature* **415**, 412–416 (2002).
- [21] Gomes, K., Pasupathy, A. N., Pushp, A., Ono, S., Ando, Y., and Yazdani, A. Visualizing pair formation on the atomic scale in the high- T_c superconductor $\text{Bi}_2\text{Sr}_2\text{CaCu}_2\text{O}_{8+\delta}$. *Nature* **447**, 569–572 (2007).
- [22] Crane, R. W., Armitage, N. P., Johansson, A., Sambandamurthy, G., Shahar, D., and Grüner, G. Fluctuations, dissipation, and nonuniversal superfluid jumps in two-dimensional superconductors. *Physical Review B* **75**(9), 094506 (2007).
- [23] Blankenbecler, R., Scalapino, D. J., and Sugar, R. L. Monte Carlo calculations of coupled boson-fermion systems. I. *Physical Review D* **24**(8), 2278–2286 (1981).
- [24] Gubernatis, J. E., Jarrell, M., Silver, R. N., and Sivia, D. S. Quantum Monte Carlo simulations and maximum entropy: Dynamics from imaginary-time data. *Physical Review B* **44**(12), 6011–6029 (1991).
- [25] Sandvik, A. W. Stochastic method for analytic continuation of quantum Monte Carlo data. *Physical Review B* **57**(17), 10287–10290 (1998).
- [26] Scalapino, D. J., White, S. R., and Zhang, S. Insulator, metal, or superconductor: The criteria. *Physical Review B* **47**(13), 7995–8007 (1993).
- [27] Trivedi, N., Scalettar, R. T., and Randeria, M. Superconductor-insulator transition in a disordered electronic system. *Phys. Rev. B* **54**(6), R3756–R3759 (1996).
- [28] Fisher, M. P. A., Weichman, P. B., Grinstein, G., and Fisher, D. S. Boson localization and the superfluid-insulator transition. *Physical Review B* **40**(1), 546–570 (1989).
- [29] Finkel'stein, A. M. Suppression of superconductivity in homogeneously disordered systems. *Physica B* **197**, 636–648 (1994).
- [30] Emery, V. J. and Kivelson, S. A. Importance of phase fluctuations in superconductors with small superfluid density. *Nature* **374**(6521), 434–437 (1995).
- [31] Sacepe, B., Dubouchet, T., Chapelier, C., Sanquer, M., Ovidia, M., Shahar, D., Feigel'man, M., and Ioffe, L. Localization of preformed Cooper pairs in disordered superconductors. *Nature Physics* **7**(3), 239–244 (2011).
- [32] Sacépé, B., Chapelier, C., Baturina, T. I., Vinokur, V. M., Baklanov, M. R., and Sanquer, M. Pseudogap in a thin film of a conventional superconductor. *Nature Communications* **1**, 140 (2010).
- [33] Mondal, M., Kamlapure, A., Chand, M., Saraswat, G., Kumar, S., Jesudasan, J., Benfatto, L., Tripathi, V., and Raychaudhuri, P. Phase fluctuations in a strongly disordered s-wave NbN superconductor close to the metal-insulator transition. *Physical Review Letters* **106**, 047001 (2011).
- [34] Hetel, I., Lemberger, T. R., and Randeria, M. Quantum critical behaviour in the superfluid density of strongly underdoped ultrathin copper oxide films. *Nature Physics* **3**(10), 700–702 (2007).

Supplementary Information for: Single and two-particle energy gaps across the disorder-driven superconductor-insulator transition

Karim Bouadim, Yen Lee Loh, Mohit Randeria, and Nandini Trivedi
Department of Physics, The Ohio State University, Columbus, OH 43210, USA

In this supplement we provide details of the determinantal QMC simulations, comparison between QMC and inhomogeneous Bogoliubov-de Gennes (BdG) mean-field theory, and the analytic continuation procedure for extracting real frequency information from imaginary time QMC data.

Determinantal QMC: We use the determinantal Quantum Monte Carlo (QMC) algorithm [1, 2] to calculate the quantities discussed in the paper, including the imaginary-time Green function $G(\mathbf{R}; \tau) = -\langle \mathcal{T}_\tau c_{\mathbf{R}\sigma}(\tau) c_{\mathbf{R}\sigma}^\dagger(0) \rangle$ and pairing correlation function $P(\tau) = \sum_{\mathbf{R}} \langle \mathcal{T}_\tau F(\mathbf{R}; \tau) F^\dagger(\mathbf{R}; 0) \rangle$ where $F(\mathbf{R}, \tau) = c_{\mathbf{R}\downarrow}(\tau) c_{\mathbf{R}\uparrow}(\tau)$. We present results for 8×8 square lattices with periodic boundary conditions. The lattice size is dictated by the need for very accurate QMC data required for analytic continuation.

For a given set of parameters, the simulations are equilibrated for up to 4×10^5 Monte Carlo steps. The final averages for a single disorder realization are taken over 2×10^5 steps for static quantities and over 4×10^6 for dynamical quantities. We further average over 10 disorder realizations for a given disorder strength. The resulting maximum absolute errors are $\delta G(\tau) \sim 10^{-4}$ and $\delta P(\tau) \sim 10^{-2}$. We have checked the main features in the density of states – the hard gap at all V , and the coherence peaks for $V \lesssim V_c$ – using extensive simulations with an average over 100 disorder realizations (Fig. 1).

Comparisons of QMC with BdG: In Fig. 2 we show a comparison of the local density $n(\mathbf{R})$ obtained using QMC and self-consistent BdG, including inhomogeneous Hartree shifts, for one disorder pattern at different disorder strengths. The close agreement indicates that phase fluctuations, not included in BdG, have very little effect on $n(\mathbf{R})$. On the other hand, the superfluid stiffness and spectral properties at finite temperatures and large disorder are greatly affected by thermal and quantum phase fluctuations.

The local density is directly related to the occupied and unoccupied part of the LDOS (see Fig. 4 of the paper) via the sum rules: $2 \int_{-\infty}^{\infty} d\omega f(\omega) N(\mathbf{R}, \omega) = n(\mathbf{R})$ and $2 \int_{-\infty}^{\infty} d\omega [1 - f(\omega)] N(\mathbf{R}, \omega) = 2 - n(\mathbf{R})$, where $f(\omega)$ is the Fermi function and the factor of 2 comes from spin degeneracy. We have tested these sum rules for the calculated LDOS and find excellent agreement. Further sum rule tests are described below.

Analytic continuation for Green's function: We use the maximum entropy method (MEM) to extract the

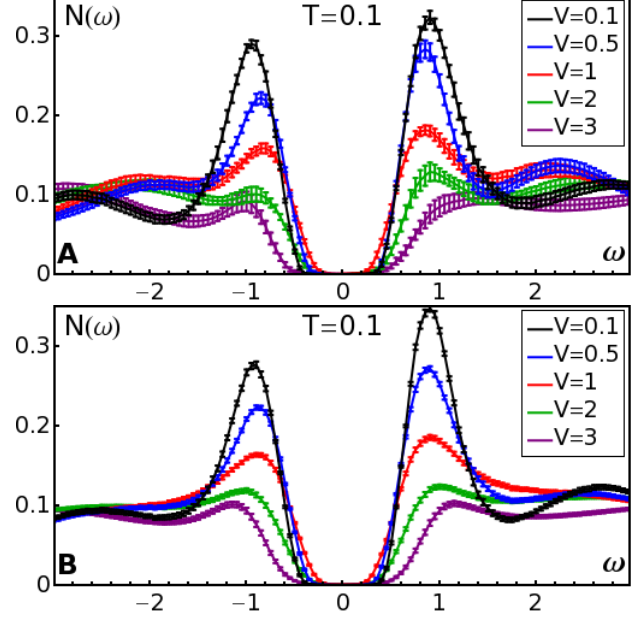


FIG. 1: Comparison of results for the density of states averaged over (A) 10 and (B) 100 disorder realizations. The main features, i.e., hard gaps for all disorder strengths and coherence peaks for $V < V_c$, are robust. Note the reduced statistical fluctuations in panel B with the increase in the number of disorder realizations.

local density of states $N(\mathbf{R}, \omega)$ from the imaginary-time Green function $G(\mathbf{R}; \tau)$. The MEM for analytic continuation [3] essentially inverts the Laplace transform

$$G(\mathbf{R}; \tau) = - \int_{-\infty}^{\infty} d\omega \frac{e^{-\tau\omega}}{1 + e^{-\beta\omega}} N(\mathbf{R}, \omega). \quad (1)$$

The average DOS $N(\omega)$ is obtained from analytic continuation of $\sum_{\mathbf{R}} G(\mathbf{R}, \tau)$.

We have performed extensive tests using known model spectra as follows: (i) choose a test spectrum $N(\omega)$; (ii) perform a Laplace transform to obtain the imaginary-time Green function $G(\tau)$; (iii) add random numbers $\delta G(\tau)$ drawn independently from a normal distribution of width $\delta G = 10^{-4}$, in order to simulate Monte Carlo statistical error; and finally (iv) feed the resulting noisy data, $G_{\text{data}}(\tau)$, into our MEM routine. This procedure is illustrated in Fig. 3. We have concluded that the MEM is adequate for extracting the low-energy features of the spectrum, particularly the gap.

Sum rules: We have also made extensive sum-rule checks for the spectra obtained from MEM. We define

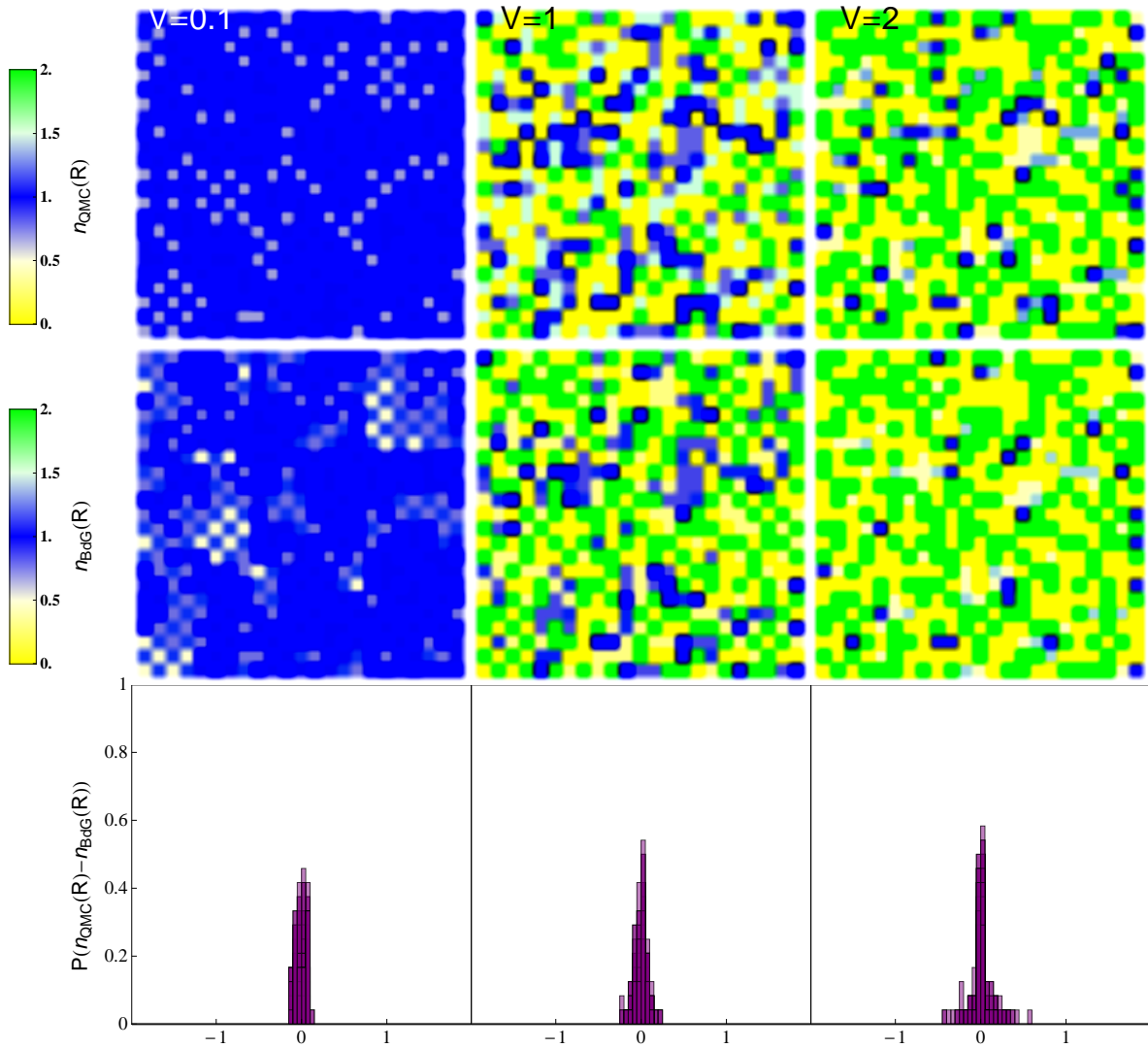


FIG. 2: Comparison of the local density $n(\mathbf{R})$ obtained using QMC (top panels) and self-consistent BdG (middle panels) for one disorder pattern at three different disorder strengths. The densities are very similar as seen from the histograms of their differences in the lowest panels, indicating that phase fluctuations have very little effect on $n(\mathbf{R})$.

$M_{\mathbf{R}}^{(m)}$, the m th frequency moment of the local density of states at position \mathbf{R} , as

$$M_{\mathbf{R}}^{(m)} = \int_{-\infty}^{\infty} d\omega \omega^m N(\mathbf{R}, \omega). \quad (2)$$

These moments satisfy the following sum rules, which can be derived rigorously by extending the analysis in Ref. [4] to a disordered system:

$$M_{\mathbf{R}}^{(0)} = 1, \quad (3)$$

$$M_{\mathbf{R}}^{(1)} = V_{\mathbf{R}} - \mu + \frac{U}{2} \langle n_{\mathbf{R}} \rangle, \quad (4)$$

$$M_{\mathbf{R}}^{(2)} - M_{\mathbf{R}}^{(1)2} = zt^2 + \frac{U^2}{4} [2 \langle n_{\mathbf{R}} \rangle - \langle n_{\mathbf{R}} \rangle^2], \quad (5)$$

where $z = 4$ is the coordination number. Differentiating Eq. (1) shows that the moments are also related to the

values and derivatives of the Green function at $\tau = 0$ and $\tau = \beta$,

$$M_{\mathbf{R}}^{(m)} = (-1)^m \left[\frac{\partial^m G_{\mathbf{R}}}{\partial \tau^m}(0) + \frac{\partial^m G_{\mathbf{R}}}{\partial \tau^m}(\beta) \right]. \quad (6)$$

QMC simulations produce very accurate results for $G_{\mathbf{R}}(0)$ and $G_{\mathbf{R}}(\beta)$, with absolute errors of about 10^{-5} . The MEM analytic continuation procedure fits these data points to within the error bars. We have verified that the MEM LDOS satisfies the moment sum rules with a fractional error of less than 0.001% for $M^{(0)}$, less than 1% for $M^{(1)}$, and about 1% for $M^{(2)}$. In contrast, the LDOS obtained from BdG calculations is found to violate the sum rules.

Analytic continuation for pairing correlation: The pair spectrum $P''(\omega)$ is related to the pairing corre-

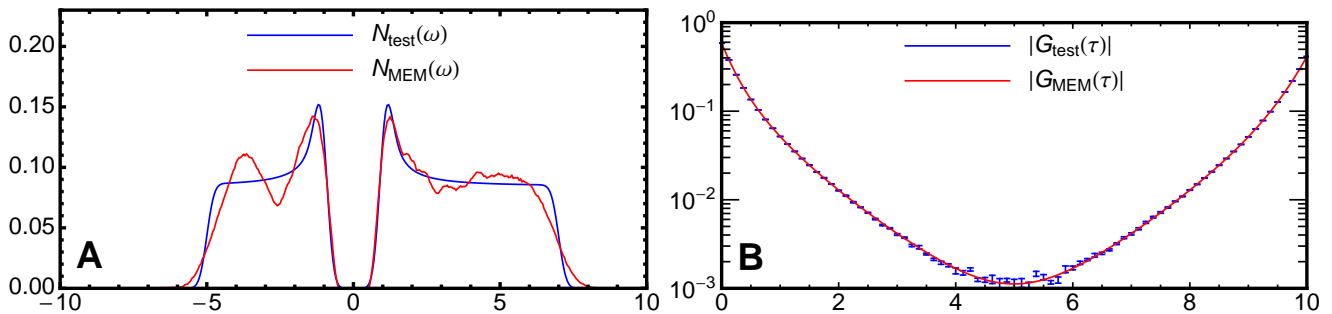


FIG. 3: Demonstration of analytic continuation using the maximum entropy method (MEM). (A) A test spectrum (blue) is chosen, noise is added in the τ -domain, and the MEM is used to reconstruct the spectrum (red). The reconstructed spectrum $N_{\text{MEM}}(\omega)$ agrees well with the test spectrum $N(\omega)$ at low energies, reproducing the correct gap structure, although there are deviations at higher energies. (B) The reconstructed Green function $G_{\text{MEM}}(\tau)$ fits the “data” $G_{\text{data}}(\tau)$ to within its error bars. The magnitude of the gap in $N(\omega)$ can be estimated by examining the exponential decay constant of $G(\tau)$, even without using the MEM.

lation function $P(\tau)$ via

$$P(\tau) = \int_{-\infty}^{\infty} \frac{d\omega}{\pi} \frac{e^{-\tau\omega}}{1 - e^{-\beta\omega}} P''(\omega). \quad (7)$$

We write this in a manner similar to the fermionic result of Eq. (1) as

$$P(\tau) = \int_{-\infty}^{\infty} \frac{d\omega}{\pi} \frac{e^{-\tau\omega}}{1 + e^{-\beta\omega}} P''(\omega) \coth \frac{\beta\omega}{2}. \quad (8)$$

and use MEM to invert the Laplace transform.

We have made extensive checks on the MEM results for $P''(\omega)$. As an example, we illustrate in Fig. 4 how very simple analytic expressions fit to the $P(\tau)$ QMC data can give us confidence in the ability of MEM to discriminate between gapped and gapless spectra. We show in the left panel of Fig. 4 the two-particle Green function $P(\tau)$ at two disorder strengths $V = 0.1$ (superconducting state) and $V = 2.8$ (insulating state). The QMC data are at low temperature $T = 0.1$ and averaged over 10 disorder realizations in each case, with error bars suppressed for clarity. At strong disorder the QMC data can be fit by an exponential decay in imaginary time (with periodicity β). This leads to a spectrum with two delta functions $P''(\omega)/\omega \propto \delta(\omega - \Omega) + \delta(\omega + \Omega)$ with $\Omega = 0.69$. At weak disorder the data can be fit better with a gapless, Lorentzian-like spectrum

$$\frac{P''(\omega)}{\omega} \propto \frac{1}{\omega} \tanh \frac{\beta\omega}{2} \times \begin{cases} \frac{1}{1+\omega^2/\Omega_+^2} & \omega > 0 \\ \frac{1}{1+\omega^2/\Omega_-^2} & \omega < 0. \end{cases} \quad (9)$$

The fact that $\Omega_+ = 1.4$ and $\Omega_- = 0.8$ in this simple fit shows the particle-hole asymmetry evident in $P(\tau)$. We emphasize that in both cases, these simple functional forms capture the essential characteristics – gapped vs. gapless – of the MEM spectrum as illustrated in the right panel of Fig. 4.

We show in greater detail in Figure 5 how $P(\tau)$ and the corresponding MEM spectra $P''(\omega)/\omega$ evolve with increasing disorder strengths. These data are averaged over 10 disorder realizations in each case. As remarked in the main text, the main trend is qualitatively clear: $P''(\omega)/\omega$ has a single peak in the superfluid state, which splits into two peaks in the insulating state ($V \gtrsim 1.6$) that separate with increasing disorder.

-
- [1] White, S. R., Scalapino, D. J., Sugar, R. L., Loh, E. Y., Gubernatis, J. E., and Scalettar, R. T. Numerical study of the two-dimensional Hubbard model. *Physical Review B* **40**(1), 506 (1989).
 - [2] Blankenbecler, R., Scalapino, D. J., and Sugar, R. L. Monte Carlo calculations of coupled boson-fermion systems. I. *Physical Review D* **24**(8), 2278–2286 (1981).
 - [3] Sandvik, A. W. Stochastic method for analytic continuation of quantum Monte Carlo data. *Physical Review B* **57**(17), 10287–10290 (1998).
 - [4] White, S. R. Spectral weight function for the two-dimensional Hubbard model. *Physical Review B* **44**(9), 4670 (1991).

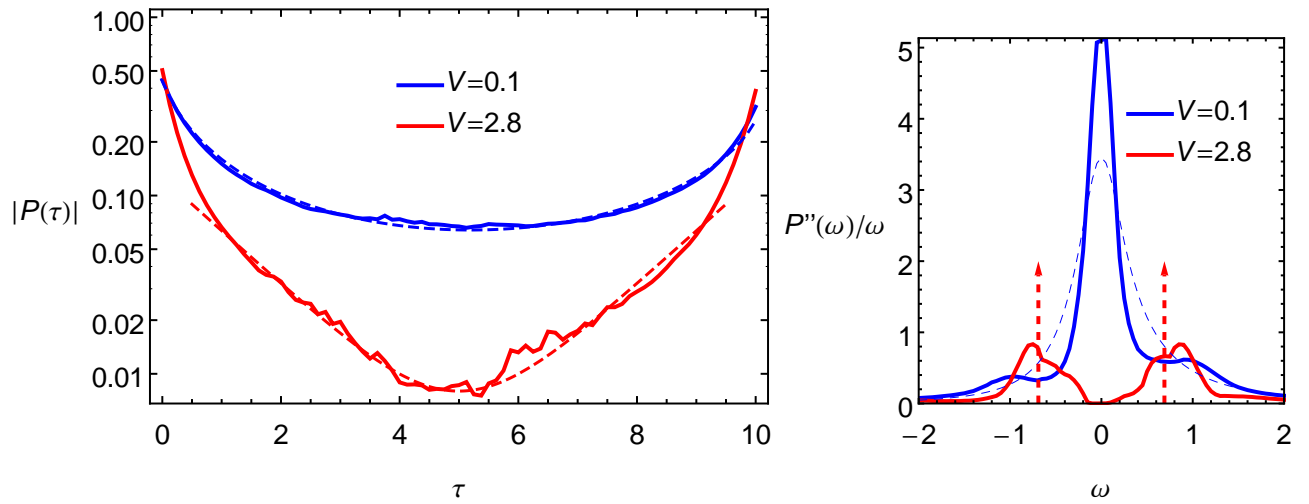


FIG. 4: (Left) Two-particle imaginary-time Green functions from QMC (each averaged over 10 disorder realizations). For strong disorder (solid red curve) the curves contain straight-line sections, i.e., regions of exponential behavior, suggesting a gapped spectrum, whereas for weak disorder there is no clear straight-line behavior. Dashed curves correspond to model spectra in right panel. (Right) Solid curves are two-particle spectra extracted using maximum entropy method. The dashed blue curve is a gapless, Lorentzian-like spectrum. The dashed red curve is a gapped spectrum.

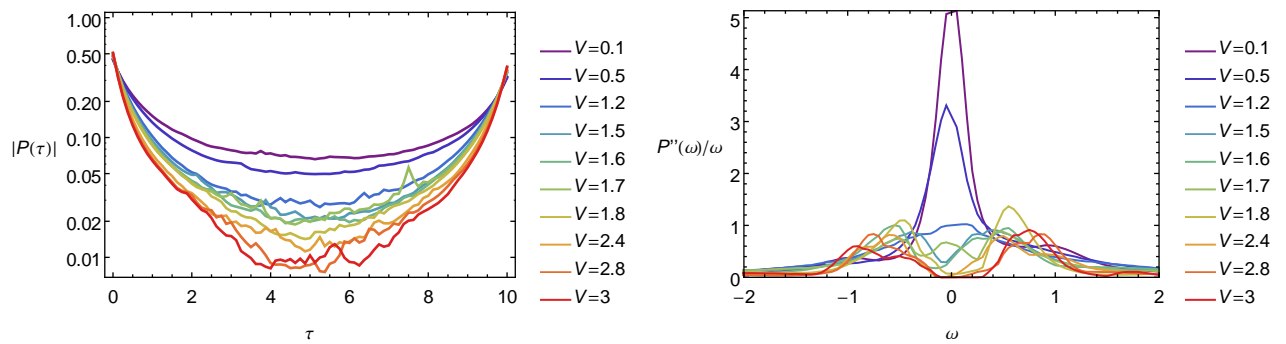


FIG. 5: (Left) Two-particle imaginary time Green function from QMC for various disorder strengths (averaged over 10 seeds). (Right) Corresponding spectra from MEM.